a rare-earth ion and of W by Nb, (*d*) substitution of W by Ti, and (*e*) substitution of W by Ta. A total of about 40 such compounds related to $Na_5W_3O_9F_5$ has been prepared and each has been shown to undergo a phase transition at which P_s vanishes and the ferroelastic–ferroelectric domain structure disappears.

References

ABRAHAMS, S. C. (1988). *Acta Cryst.* B**44**, 585–595.

ABRAHAMS, S. C., BERNSTEIN, J. L., CHAMINADE, J. P. & RAVEZ, J. (1983). *J. Appl. Cryst.* **16**, 96–98.

ABRAHAMS, S. C., IHRINGER, J. & MARSH, P. (1989). *Acta Cryst.* B**45**, 26–34.

ABRAHAMS, S. C., IHRINGER, J., MARSH, P. & NASSAU, K. (1984). *J. Chem. Phys.* **81**, 2082–2087.

ABRAHAMS, S. C., KURTZ, S. K. & JAMIESON, P. B. (1968). *Phys. Rev.* **172**, 551–553.

ABRAHAMS, S. C., MARSH, P. & RAVEZ, J. (1987). *J. Chem. Phys.* **87**, 6012–6020.

ABRAHAMS, S. C., SVENSSON, C. & BERNSTEIN, J. L. (1980). *J. Chem. Phys.* **72**, 4278–4285.

AIZU, K. (1970). *J. Phys. Soc. Jpn*, **28**, 706–716.

BECKER, P. J. & COPPENS, P. (1974). *Acta Cryst.* A**30**, 129–147, 148–153.

BOND, W. L. (1960). *Acta Cryst.* **13**, 814–818.

BROSSET, C. (1938). *Z. Anorg. Allg. Chem.* **238**, 201–208.

BUSING, W. R., MARTIN, K. O. & LEVY, H. A. (1973). *J. Appl. Cryst.* **6**, 309–346.

DESLATTES, R. D. & HENINS, A. (1973). *Phys. Rev. Lett.* **31**, 972–975.

DOUMERC, J. P., ELAATMANI, M., RAVEZ, J., POUCHARD, M. & HAGENMULLER, P. (1979). *Solid State Commun.* **32**, 111–113.

Enraf–Nonius (1984). *CAD-4 Operators Manual.* Enraf–Nonius, Delft, The Netherlands.

IHRINGER, J. & ABRAHAMS, S. C. (1984). *Phys. Rev. B*, **30**, 6540–6548.

International Tables for X-ray Crystallography (1974). Vol. IV. Birmingham: Kynoch Press. (Present distributor Kluwer Academic Publishers, Dordrecht.)

JACOBONI, C., LEBLE, A. & ROUSSEAU, J. J. (1981). *J. Solid State Chem.* **36**, 297–304.

LABBÉ, PH., LELIGNY, H., RAVEAU, B., SCHNECK, J. & TOLÉDANO, J. C. (1989). Private communication.

LANDOLT-BÖRNSTEIN (1981). *Ferroelectrics and Related Substances: Oxides.* New Series III/16a. Berlin: Springer-Verlag.

LANDOLT-BÖRNSTEIN (1982). *Ferroelectrics and Related Substances: Nonoxides.* New Series III/16b. Berlin: Springer-Verlag.

RAVEZ, J., ABRAHAMS, S. C., ZYONTZ, L. E. & CHAMINADE, J. P. (1983). *Studies in Inorganic Chemistry*, edited by R. METSELAAR, H. J. M. HEIJILIGERS & J. SCHOONMAN. Amsterdam: Elsevier.

RAVEZ, J., ELAATMANI, M. & CHAMINADE, J. P. (1979). *Solid State Commun.* **32**, 749–754.

RAVEZ, J., ELAATMANI, M. & HAGENMULLER, P. (1981). *Mater. Res. Bull.* **16**, 1253–1259.

RAVEZ, J., ELAATMANI, M., HAGENMULLER, P. & ABRAHAMS, S. C. (1981). *Ferroelectrics*, **38**, 777–780.

RAVEZ, J., ELAATMANI, M., VON DER MÜHLL, R. & HAGENMULLER, P. (1979). *Mater. Res. Bull.* **14**, 1083–1087.

ROCQUET, P. & COUZI, M. (1985). *J. Phys. C*, **18**, 6571–6579.

ROCQUET, P., COUZI, M., TRESSAUD, A., CHAMINADE, J. P. & HAUW, C. (1985). *J. Phys. C*, **18**, 6555–6569.

SVENSSON, C., ABRAHAMS, S. C. & BERNSTEIN, J. L. (1979). *J. Chem. Phys.* **71**, 5191–5195.

TORRE, L. P., ABRAHAMS, S. C. & BARNS, R. L. (1972). *Ferroelectrics*, **4**, 291–298.

Acta Cryst. (1989). B**45**, 370–378

Structural Study of the Incommensurate and Lock-In Phases of Rb_2ZnCl_4

BY A. HEDOUX AND D. GREBILLE

Laboratoire de Chimie-Physique du Solide (UA 453), Ecole Centrale de Paris, 92295 Châtenay-Malabry CEDEX, France

J. JAUD

Laboratoire de Chimie de Coordination, 205 route de Narbonne, 31077 Toulouse, France

AND G. GODEFROY

Laboratoire de Physique du Solide (UA 785), Faculté des Sciences, BP 138, 21004 Dijon CEDEX, France

(*Received* 14 *October* 1988; *accepted* 11 *April* 1989)

Abstract

The crystal structures of Rb_2ZnCl_4 at 210 K [incommensurate structure, $a = 7{\cdot}253$ (5), $b = 12{\cdot}646$ (9), $c = 9{\cdot}221$ (7) Å] and 115 K [threefold commensurate superstructure, $a = 7{\cdot}230$ (5), $b = 12{\cdot}608$ (9), $c = 9{\cdot}199$ (7) Å] have been investigated from X-ray single-crystal diffraction data. The refinement program *REMOS* was used. The final *wR* factors at 210 and 115 K are respectively 0·045 and 0·041 for 1073 and 1215 main reflections, and 0·187 and 0·136 for 587 and 1065 first-order satellite reflections. The superspace groups are designated as $P(Pmcn)$:$(s,s,\bar{1})$ and $P(P2_1cn)$:$(\bar{1},s,\bar{1})$ in the incommensurate and lock-in phases, respectively. The modulation is interpreted as rotations of rigid $ZnCl_4$ tetrahedra around two cristal-

0108-7681/89/040370-09$03.00 © 1989 International Union of Crystallography

lographic directions. Calculations of polarization confirmed the choice of the superspace group in the incommensurate phase and showed a connection between the ferroelectricity of the crystal and structural elements of the threefold superstructure. The comparison of the structural results of both structures outlines the continuous character of the lock-in transition.

1. Introduction

Rb_2ZnCl_4, in common with other compounds of the A_2BX_4 family, exhibits an incommensurate phase (INC) below $T_i = 302$ K, which is characterized by its basic structure ($Pmcn$, $Z = 4$) and by the modulation wavevector $\mathbf{q}_\delta = [1/3 - \delta(T)]\mathbf{c}^*$. The cell structure of the high-temperature phase and of the basic structure of the modulated phase is shown schematically in Fig. 1. It consists of four symmetry-related groups of one $ZnCl_4$ tetrahedron and two Rb atoms. Each atom is in special position 4(c), except Cl(3) which is in a general position. A previous study (Hedoux, Grebille, Lefebvre & Perret, 1989) has shown that the temperature dependence of $\mathbf{q}$ changes with the method of the synthesis of the crystal. Consequently, the lock-in temperature T_L is connected with the crystal-growth method, and varies in the best cases in the range 182–190 K and decreases and even cannot be observed for more defective samples. At T_L, δ vanishes and the ferroelectric commensurate phase (C) is realized ($P2_1cn$, $Z = 4$).

The structure of the INC phase has been described with a split-atom model in which the Cl atoms are divided into two parts (Quilichini & Pannetier, 1983). This model improves the structure refinement as it takes artificial account of the influence of the modulation on the intensities of the basic diffraction pattern, but it introduces additional parameters and does not allow modulated atomic positions to be determined.

In order to understand the phase transitions at T_i and T_L, and properly describe the structure of the different phases and the origin of ferroelectric properties of the compound, it was necessary to determine the modulated atomic positions in the INC and C phases of the crystal. Consequently, the multidimensional approach and superspace formalism (de Wolff, Janssen & Janner, 1981) have been used to describe both phases. In particular the use of the refinement program *REMOS* (Yamamoto, 1982) allowed us to simplify drastically the analysis and the descriptions of the modulated structures.

2. Experimental

Single crystals of Rb_2ZnCl_4 were grown by slow evaporation from an aqueous solution. Spherical crystals ($d = 0{\cdot}3$ mm) were used to collect the data needed for the structure refinements of the INC and C phases. The integrated intensities were measured by the θ–2θ scan technique up to $[(\sin\theta)/\lambda]_{max} = 0{\cdot}995$ Å^{-1} (h=0–11, k=0–20, l=0–14, $m=\pm1$), with an automatic four-circle diffractometer (Enraf–Nonius CAD-4) and Mo $K\alpha$ radiation. The diffractometer was equipped with an N_2-gas-flow low-temperature system, which keeps temperature fluctuations within $\pm0{\cdot}5$ K. The cell constants of the average structures were determined by least-squares refinement of the Bragg angles of 25 main reflections. No intensity variation was observed for three standard reflections (400, 330 and 222) during the recording of the data. The data were corrected for absorption (the minimum and maximum correction factors, are 0·8446 and 0·9979, respectively, the average correction factor being 0·9244). Secondary-extinction corrections based on transfer equations derived by Kato (1976*a*,*b*) were applied.

2.1. *The INC phase*

A preliminary study of the INC phase (Hedoux *et al.*, 1989) has shown that the modulation wavevector is pinned from T_i down to a temperature T_m, dependent on the crystal-growth method. On this plateau the profiles

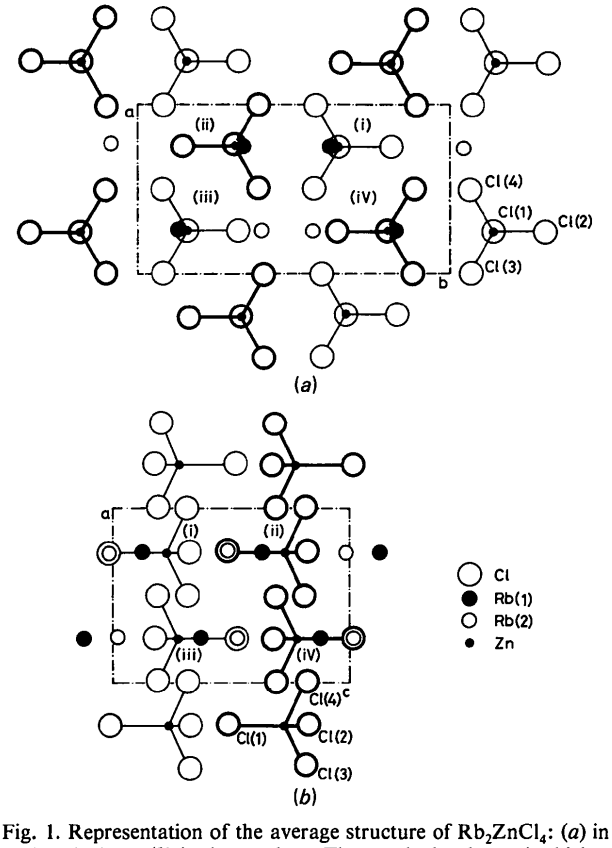

Fig. 1. Representation of the average structure of Rb_2ZnCl_4: (*a*) in the *ab* plane, (*b*) in the *ac* plane. The tetrahedra drawn in thicker lines are in the plane located at $z = 3/4$, the others being in the plane located at $z = 1/4$. Atomic positions given in Table 1 are translated by $y = 1/4$.

of the main and satellite reflections are similar. Below T_m, the nucleation of a second incommensurate phase involves the coexistence of two satellite reflections over a rather large range of temperature (about 10 K). The satellites of the new INC phase are more widened than those of the first one, and this reflects the poorer crystalline quality of this phase. Consequently, the data collection was performed on the plateau just above T_m, where the intensity of the first-order satellite reflections is maximum, where the line widths of the satellites and of the main reflections are similar, and where only one INC phase is observed. In the case of the sample used ($T_m = 200$ K), the measurements were performed at 210 K, and the wavevector of the modulation was characterized by $\delta = 0{\cdot}027$ ($\mathbf{q}_\delta = 0{\cdot}306\mathbf{c}^*$). The cell constants of the average structure are: $a = 7{\cdot}253$ (5), $b = 12{\cdot}646$ (9), $c = 9{\cdot}221$ (7) Å. 1073 main reflections and 587 first-order satellite reflections (with $I > 3\sigma$) were measured.

2.2. *The lock-in phase*

The data collection was performed at $T = 115$ K. At this temperature, the misfit parameter δ vanishes and the wavevector of the modulated structure is then $\mathbf{c}^*/3$. The cell constants were refined at this temperature: $a = 7{\cdot}230$ (5), $b = 12{\cdot}608$ (9), $c = 9{\cdot}199$ (7) Å. No intensity variation was observed for the three standard reflections. 1215 main reflections and 1065 first-order satellites (with $I > 3\sigma$) were measured.

3. Four-dimensional description of a modulated structure

A displacive INC structure corresponds to a distortion of a basic structure. Consequently, the atomic positions in the four-dimensional lattice are characterized by the modulated displacements from their average position in the basic structure. The coordinate of each atom is given by

$$x_i^\mu = \bar{x}_i^\mu + u_i^\mu \quad (i = 1, 2, 3, 4) \tag{1}$$

where $\bar{x}_i^\mu$ is the coordinate in the basic structure and u_i^μ is the displacement from $\bar{x}_i^\mu$. This displacement is a periodic function of the fourth coordinate $\bar{x}_4^\mu$ (internal coordinate), defined by the following relation:

$$\bar{x}_4^\mu = \mathbf{q}.x^\mu + t \tag{2}$$

where $\mathbf{q}$ is the modulation wavevector and t an arbitrary phase. Therefore the components of the displacement of each atom can be expressed as an expansion of a Fourier series, which is called a modulation function:

$$u_i(\bar{x}_4^\mu) = \sum_{n=1}^{l} (a_{in}^\mu \cos 2\pi n \bar{x}_4^\mu + b_{in}^\mu \sin 2\pi n \bar{x}_4^\mu) \quad (i = 1, 2, 3, 4) \tag{3}$$

where

$$a_{4n}^\mu = \sum_{i=1}^{3} q_i a_{in}^\mu, \qquad b_{4n}^\mu = \sum_{i=1}^{3} q_i b_{in}^\mu \tag{4}$$

and n is the order of the Fourier term.

In the present case, the modulation function is expanded up to the order $l = 1$, because only the first-order satellites are significant and have been measured in both phases. The Fourier amplitudes are considered as structural parameters in the refinement. The number of these parameters can be reduced by superspace symmetry considerations. If two atoms, μ and ν, are symmetry-related by $\{R/V\}$ in the basic structure, then the corresponding superspace-group element $\{R, \varepsilon/V, \tau\}$ implies the following relations:

$$x_i^\nu = \sum_{j=1}^{3} R_{ij} x_j^\mu + V_i \quad (i = 1, 2, 3)$$

$$x_4^\nu = \varepsilon x_4^\mu + \tau - \mathbf{q}.\mathbf{V} \tag{5}$$

where $\varepsilon = \pm 1$ if $R_{ij}.\mathbf{q} = \varepsilon\mathbf{q}$.

If the atoms μ are located in special positions in the basic structure, the atomic modulation functions u_i for these atoms verify the relations:

$$u_i^\mu(\bar{x}_4^\mu) = \sum_{j=1}^{4} R_{ij} u_j^\mu [R_{44}(\bar{x}_4^\mu - \tau)]. \tag{6}$$

These relations involve a special form of the modulation functions (parity or nullity of different components of the function) of atoms localized in special positons.

The form (3) of the modulation function is similar for an INC and a C structure; however, its meaning is different in each case.

In the first case (INC), there is at least one irrational component q_j of the modulation vector $\mathbf{q}$. In our case, $q_3 = 0{\cdot}306$. An atom μ_0 in the origin cell, characterized by its average position x^μ, corresponds by the translation group of the crystal to all the atoms μ_T, characterized by their average position $x^\mu + \mathbf{T}$, where $\mathbf{T}$ is a vector of the direct lattice. The argument $\mathbf{q}(\mathbf{x}^\mu + \mathbf{T})$ of the modulation function forms, modulo 1, an infinite and dense discrete set in the interval [0,1]. And so, there is always one atom in the crystal which allows any possible value of the modulation function (3) to be reached. Thus, this modulation function represents the distribution of all the modulated atomic positions over all the cells of the crystal, and each atom, in the supercrystal representation, can be considered as a continuous string along the internal direction. The variations of the phase t in the range [0,1] in (2) describe, in one cell, all the modulated positions occupied in the whole crystal. The calculation of the structure factors is then obtained by a continuous summation over the internal coordinate.

In the second case (C), all the components q_i are rational. In our case $q_3 = 1/3$ and the argument

Table 1. *Positional* ($\times 10^4$) *and equivalent isotropic thermal parameters* ($\text{Å}^2 \times 10^4$) *of the INC structure*

$$U_{eq} = (U_{11} + U_{22} + U_{33})/3.$$

		R_0	a_0	a_1	b_1	U_{eq}
Rb(1)	x	2500	0	−112 (4)	82*	
	y	4067	−3 (1)	0	0	441 (5)
	z	6298	4 (1)	0	0	
Rb(2)	x	2500	0	−19 (4)	159 (3)	
	y	8196	−3 (1)	0	0	245 (5)
	z	4862	3 (1)	0	0	
Zn	x	2500	0	31 (3)	98 (3)	
	y	4217	2 (1)	0	0	134 (5)
	z	2240	−2 (1)	0	0	
Cl(1)	x	2500	0	73 (13)	413 (10)	
	y	4189	1 (3)	0	0	389 (13)
	z	−175	−3 (3)	0	0	
Cl(2)	x	2500	0	549 (9)	68 (13)	
	y	5851	−3 (2)	0	0	336 (14)
	z	3204	6 (3)	0	0	
Cl(3)	x	10	9 (3)	−197 (6)	48 (6)	
	y	3410	−10 (3)	279 (4)	−1 (6)	363 (18)
	z	3139	−7 (3)	136 (6)	−101 (6)	

* Not refined to fix the phase origin.

$\mathbf{q}(\mathbf{x}^\mu + \mathbf{T})$ can only take the values $\mathbf{q}.\mathbf{x}^\mu$, $\mathbf{q}.\mathbf{x}^\mu + 1/3$ and $\mathbf{q}.\mathbf{x}^\mu + 2/3$, modulo 1. There are only three particular possible values of the modulation functions, which describe three modulated positions periodically occupied in all three cells. The structure factors are then calculated, with the contribution of these three values of the phase t in the range [0,1], by a discrete summation over the internal coordinate, and in the supercrystal representation, there are only three points of the preceding continuous string which represent real atomic positions in the crystal.

4. Refinement of the structures

The refinement of both structures was performed using the *REMOS* program (Yamamoto, 1982). It minimizes the reliability factor wR:

$$wR = \sum_i w_i (F_{oi} - F_{ci})^2 / \sum_i w_i F_{oi}^2,$$

where w_i is a weighting factor, and F_{oi} and F_{ci} are the observed and calculated structure factors. Unit weights were used for all reflections. The atomic scattering factors were taken from *International Tables for X-ray Crystallography* (1974).*

4.1. *The INC phase*

Dielectric constant measurements (Hamano, Ikeda, Fujimoto, Ema & Hirotsu, 1980; Hamano, Sakata & Ema, 1985) present a very weak anomaly at T_i. Studies of the permittivity constant (Fousek & Kroupa, 1987) and spontaneous polarization (Shuvalov, Gridnev, Prasolov & Sannikov, 1988; Sawada, Shiroishi, Yamamoto, Takashige & Matsuo, 1977) also tend to confirm that the point group of the basic structure of the INC phase is nonpolar and is the same as the group of the high-temperature phase, *Pmcn*. Taking into account the extinction rules observed for the diffraction pattern (de Wolff *et al.*, 1981):

$$m = 2n \quad \text{for} \quad (0, k, l, m)$$
$$l + m = 2n \quad \text{for} \quad (h, 0, l, m)$$
$$k + l = 2n \quad \text{for} \quad (h, k, 0, m),$$

the superspace group is designated as $P(Pmcn)$:$(s,s,\bar{1})$ in accordance with de Wolff's notation (de Wolff *et al.*, 1981) and as $(2^{\blacktriangledown}_{a+b} \perp 2_c, m_{c+d}, m_d)$ in accordance with WPV notation (Grebille, Weigel, Veysseyre & Phan, 1989). The superspace-group elements are:

$$\{E/(0,0,0),0\} \qquad \{I/(0,0,0),0\}$$
$$\{\sigma_x/(\tfrac{1}{2},0,0),\tfrac{1}{2}\} \qquad \{C_{2x}/(\tfrac{1}{2},0,0),\tfrac{1}{2}\}$$
$$\{\sigma_y/(0,\tfrac{1}{2},\tfrac{1}{2}),\tfrac{1}{2}\} \qquad \{C_{2y}/(0,\tfrac{1}{2},\tfrac{1}{2},),\tfrac{1}{2}\}$$
$$\{\sigma_z/(\tfrac{1}{2},\tfrac{1}{2},\tfrac{1}{2}),0\} \qquad \{C_{2z}/(\tfrac{1}{2},\tfrac{1}{2},\tfrac{1}{2}),0\}.$$

In the basic structure, the cell is generated by six atoms (given in Table 1). Of these, five are located in special positions on the mirror plane σ_x.

The seventh atom of group 1 is generated from the atom Cl(3) (which is in a general position) by the symmetry operation σ_x. The three other groups in the cell are generated from the group (i) by:

$$\{\sigma_y/(0,\tfrac{1}{2},\tfrac{1}{2}),\tfrac{1}{2}\} \qquad \text{(group ii)}$$
$$\{\sigma_z/(\tfrac{1}{2},\tfrac{1}{2},\tfrac{1}{2}),0\} \qquad \text{(group iii)}$$
$$\{C_{2x}/(\tfrac{1}{2},0,0),\tfrac{1}{2}\} \qquad \text{(group iv)}$$

The expansion of the modulation function up to the order 1 gives 54 positional parameters, the first-order harmonic being described by its real (cosine) and imaginary (sine) parts. The restrictions (6) were applied to the five atoms located on the mirror plane. Consequently, the first average coordinate and the second and third coordinate of the Fourier terms are fixed to 0. The number of positional parameters is then reduced to 29. Only zero-order harmonics of the 26 anisotropic thermal parameters are considered; a total of 55 parameters were used to describe the INC structure. The final wR factors were respectively 0·045 and 0·187 for the main and satellite reflections, and 0·060 for all the reflections. The fitted values of the parameters are given in the Table 1.

From (3) and the fitted values of the positional parameters, three modulation functions (depending on the internal coordinate) were calculated and schematically drawn (Fig. 2). They represent the atomic

* Lists of structure factors and anisotropic thermal parameters have been deposited with the British Library Document Supply Centre as Supplementary Publication No. SUP 51784 (42 pp.). Copies may be obtained through The Executive Secretary, International Union of Crystallography, 5 Abbey Square, Chester CH1 2HU, England.

displacements from the average positions for t in the range [0,1]. They can be described in a single cell by an elliptic 'trajectory' (Fig. 3) which has no physical reality for one particular atom, but corresponds to real displacements reached in the different cells of the whole crystal by all the equivalent atoms.

Table 1 and Figs. 2 and 3 show that the incommensurate distortion is essentially due to the atomic modulation of Cl atoms. The variations of interatomic distances Zn_i—Cl_i and Cl_i—Cl_i as a function of the phase t (Fig. 4) show that the $ZnCl_4$ tetrahedra can be treated, to a good approximation, as rigid bodies. Consequently, the displacements of Zn and Cl atoms from their average positions were reduced to a global translational movement and to three independent rotations around the crystallographic directions, by a least-squares refinement program. These calculations have pointed out two significant rotations around the **b** and **c** directions; the maximum values reached by the rotations are 5·1 and 10·2°, respectively. These results are in agreement with the rotations symbolized by the elliptic trajectory drawn in Fig. 3. The modulated rotations R_y and R_z are shown in Fig. 5 as function of the phase t.

The rotations of the four tetrahedra of a cell are symmetry-related. In order to characterize these rotations, they have been schematically drawn in two planes perpendicular to the two rotation axes (Fig. 6) and interatomic Cl—Cl distances have been calculated between two neighbouring tetrahedra (Table 2). It is clear that the most important rotation is around the **c** direction, the rotations of the tetrahedra around this axis being in phase. In the plane *ac* no evident connection of phase has been observed between the four tetrahedra rotations around the **b** direction.

Table 2 shows that shorter interatomic distances present the weaker variations. This finding outlines the physical coherence of the refinement results.

To determine an eventual correlation between the rotations of the tetrahedra and the modulated displace-

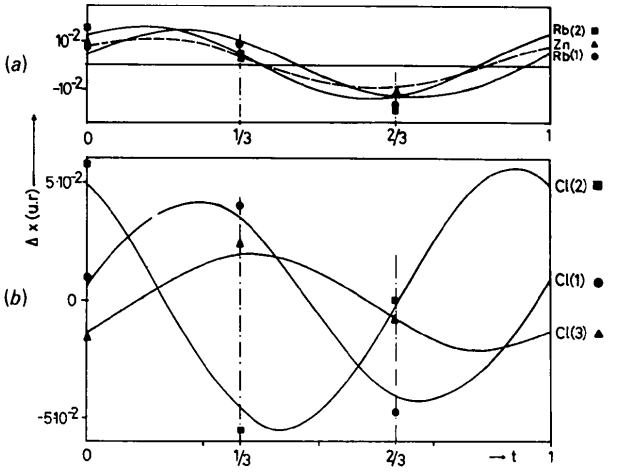

Fig. 2. Atomic displacement modulation functions along the x axis of (*a*) Zn and Rb atoms and (*b*) Cl atoms in the INC structure. The discrete points represent the corresponding displacements in the lock-in structure.

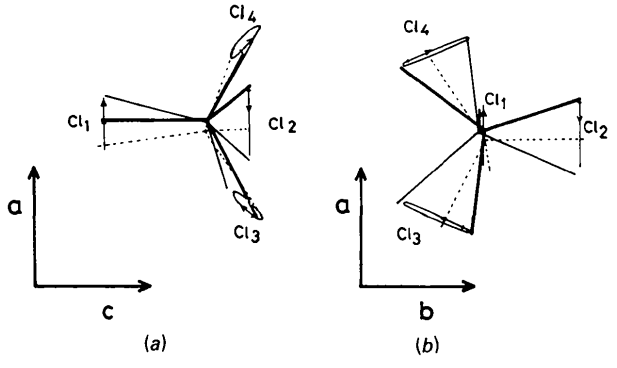

Fig. 3. Representation in the *ac* plane (*a*) and the *ab* plane (*b*) of the different possible positions of one tetrahedron in the INC phase. The Zn—Cl bonds are drawn for the three modulated positions of the tetrahedron in the superstructure (—, $t = 0$; —, $t = 1/3$; ---, $t = 2/3$). The atomic displacements are doubled to give a better observation.

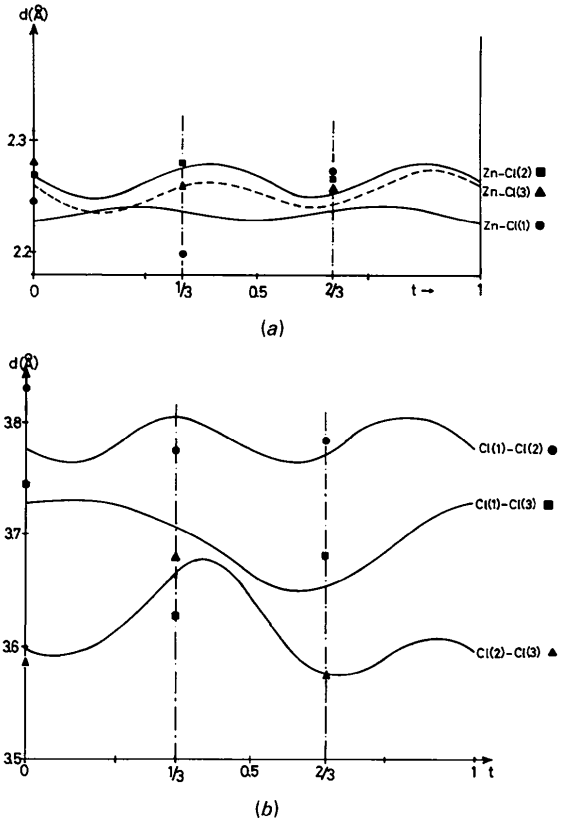

Fig. 4. Interatomic Zn—Cl distances (*a*) and Cl—Cl distances (*b*) as a function of the internal coordinate. The discrete points represent the variations of these interatomic distances in the superstructure.

ments along the **a** direction of the Rb atoms, interatomic distances Rb(1)—Cl and Rb(2)—Cl were calculated (Table 3). These calculations show that the variations of Rb(2)—Cl distances are weaker than those of Rb(1)—Cl distances, which tends to confirm that Rb(2)—Cl bonds are more rigid than Rb(1)—Cl bonds. This result is in agreement with the fact that the Rb(2) atoms are situated in smaller Cl cages than the Rb(1) atoms. So, Rb(1) atoms have more space to move, which can be also related to the stronger values of the temperature factors. The same effect was observed by Quilichini & Pannetier (1983).

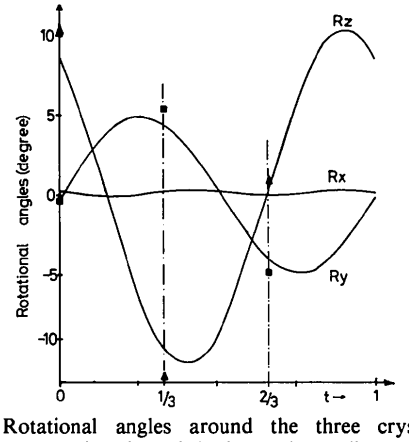

Fig. 5. Rotational angles around the three crystallographic directions as a function of the internal coordinate. The discrete points represent the three possible rotational angles of one tetrahedron in the superstructure.

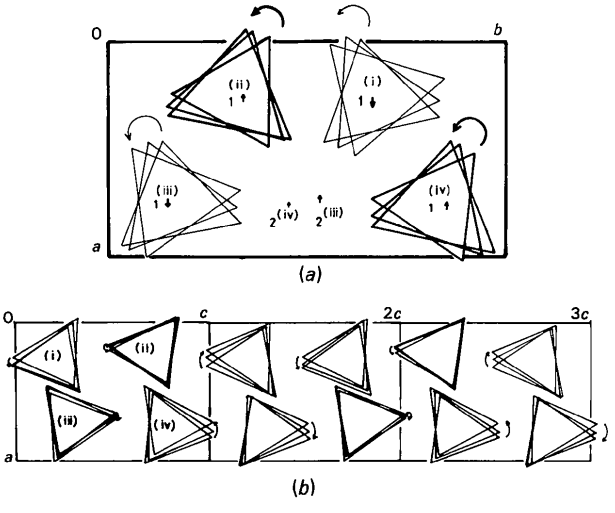

Fig. 6. Schematic representation of $ZnCl_4$ rigid-body tetrahedra. (*a*) In the *ab* plane; *t* takes the values 0, 0·125, 0·250. The arrows represent the modulated displacement of Rb atoms. The tetrahedra drawn in thicker lines are localized in layers normal to **c** at about $z = 3/4$. The others belong to the layers localized at about $z = 1/4$. Atomic positions given in Table 1 are translated by $y = 1/4$. (*b*) In the *ac* plane; *t* takes the same values (0, 0·125, 0·250) in three successive cells along **c**. To clarify the drawing the modulated displacements are doubled.

Table 2. *Interatomic* Cl—Cl *distances* (Å) *between two neighbouring tetrahedra*

	d_{max}	d_{min}	Δd
Cl(4^{i})–Cl(1^{ii})	4·312	3·805	0·507
Cl(4^{i})–Cl(4^{ii})	5·498	4·795	0·703
Cl(4^{i})–Cl(2^{iii})	4·044	3·851	0·193
Cl(4^{i})–Cl(2^{iv})	4·104	3·825	0·279
Cl(4^{i})–Cl(3^{i})	3·676	3·604	0·072
Cl(1^{ii})–Cl(1^{iii})	4·252	4·104	0·148
Cl(1^{ii})–Cl(2^{iii})	5·093	4·099	0·994
Cl(1^{ii})–Cl(3^{iii})	4·670	4·291	0·379
Cl(2^{i})–Cl(2^{iv})	5·859	4·896	0·963

Table 3. *Interatomic* Rb—Cl *distances* (Å)

	d_{max}	d_{min}	Δd
Rb(1^{i})–Cl(1^{i})	3·268	3·250	0·018
Rb(1^{i})–Cl(2^{i})	3·661	3·635	0·026
Rb(1^{i})–Cl(3^{i})	3·714	3·374	0·340
Rb(1^{i})–Cl(1^{ii})	4·352	4·336	0·016
Rb(1^{i})–Cl(3^{ii})	4·414	3·536	0·878
Rb(1^{i})–Cl(2^{iv})	3·964	3·348	0·616
Rb(1^{i})–Cl(3^{iv})	4·148	3·308	0·840
Rb(2^{iv})–Cl(4^{i})	3·349	3·266	0·083
Rb(2^{iv})–Cl(1^{ii})	4·245	3·461	0·784
Rb(2^{iv})–Cl(4^{ii})	3·375	3·316	0·059
Rb(2^{iv})–Cl(1^{iii})	3·335	3·309	0·026
Rb(2^{iv})–Cl(2^{iii})	3·333	3·316	0·017
Rb(2^{iv})–Cl(2^{iv})	3·356	3·335	0·021

Fig. 6 suggests that the modulated displacement along **a** of Rb(2^{iv}) is connected with the rotation around **c** of the tetrahedra $ZnCl_4^{iii}$, the modulation functions of Rb(2^{iv}) and Cl(2^{iii}) atoms being nearly in phase along **a**. Moreover, Fig. 6(*a*) indicates also that the displacement of Rb(1^{i}) along **a** could be connected with the rotation around **c** of the tetrahedra $ZnCl_4^{iv}$. In the plane *ac* (Fig. 6*b*), no evident phase relation between tetrahedra rotations and displacements of Rb atoms has been observed.

The average atomic positions given in Table 1 are similar to those determined by Quilichini & Pannetier (1983) in the average structure of the INC phase. But the split-atom model presents several imperfections:

(*a*) The Rb atoms are fixed in their average positions and, consequently, the role of these atoms in the incommensurate behaviour and also in the realization of the physical properties is neglected.

(*b*) The displacements of the Cl atoms from their average positions are calculated as average displacements which are similar for all equivalent Cl atoms. In reality, these displacements are modulated and the modulated displacement depends on the localization of each atom in the crystal.

However, the positions of these Cl atoms, determined from the split-atom model, are relatively coherent with our results, and give an approximate description of the incommensurate behaviour and of the amplitudes of the modulated displacements.

4.2. *The lock-in phase*

The physical measurements, quoted in §4.1 have shown the realization of the ferroelectric state at 190 K,

with a spontaneous polarization along the **a** axis of the paraelectric phase. The point group of the basic structure is the polar group $P2_1cn$ and the superspace group is $P(P2_1cn)$:$(\bar{1},s,\bar{1})$ in de Wolff's notation and $2^{\blacktriangledown}_{a+b}/m_{c+d}$, $\bar{1}^{\blacktriangledown}_{a}$ in the WPV notation; it contains the following four elements:

$$\{(E/0,0,0),0\};$$
$$\{(C_{2x}/\tfrac{1}{2},0,0),\tfrac{1}{2}\};$$
$$\{(\sigma_y/0,\tfrac{1}{2},\tfrac{1}{2}),\tfrac{1}{2}\};$$
$$\{(\sigma_z/\tfrac{1}{2},\tfrac{1}{2},\tfrac{1}{2}),0\}.$$

In this phase, all atoms are located in a general position and the unit cell is generated by seven atoms. The structure is described by 63 positional parameters (zero and first order of Fourier terms) and 42 anisotropic thermal parameters (zero order of Fourier terms). The data were treated by the *REMOS* refinement program. The final R factors are 0·041 and 0·136 for 1215 main reflections and 1065 first-order satellite reflections, respectively, and 0·0587 for all reflections. The fitted parameters are given in Table 4 and the results are shown schematically in Figs. 2–5 by discrete points or lines. These values define three particular modulated atomic positions occupied in three consecutive cells, which generate the whole crystal.

4.3. *Comparison of the structures*

Given the description of both phases with the four-dimensional concept, the two structures can be directly compared. A comparison of Tables 1 and 4 shows a decrease of thermal parameters and an increase of modulated displacements in the lock-in phase in agreement with theoretical considerations. However, the thermal parameters of Rb atoms can be considered as abnormally large [Rb(1), in particular] with the same ratio in both phases. This can be interpreted by a distortion still stronger than the one described by the modulation function, or which is not correctly described by only one order of Fourier modulation terms.

In Figs. 2 and 3, the three particular modulated positions [determined from (3) and corresponding to the lock-in value $\mathbf{c}^*/3$ of the modulation wavevector] of each atom are compared with the atomic displacement modulation function. These figures compensate for the weak increase of the distortion below T_c and show the agreement between the two structures.

The weak variations in interatomic distances (Cl^i–Cl^i and Zn^i–Cl^i) observed in Fig. 4 mean that three orientations of the tetrahedra around **b** and **c** (out of an infinite number occupied in the INC phase) are possible, and we can always describe the displacements of the $ZnCl_4$ tetrahedra as rigid-body motions (Fig. 5).

The striking difference between the two phases is the relative shift along **a** of the average positions of the Rb(1) atoms in the lock-in phase (Table 4) in relation to all the other atoms of the cell.

Table 4. *Positional* ($\times 10^4$) *and equivalent isotropic thermal parameters* ($Å^2 \times 10^4$) *of the superstructure*

$$U_{eq} = (U_{11} + U_{22} + U_{33})/3.$$

		R_0	a_0	a_1	b_1	U_{eq}
Rb(1)	x	2500	−6*	−116*	123 (3)	
	y	4067	−8 (1)	15 (4)	46 (4)	289 (11)
	z	6298	−9 (1)	−17 (4)	14 (5)	
Rb(2)	x	2500	−76 (7)	−21 (3)	202 (2)	
	y	8196	−5 (1)	−13 (3)	5 (3)	153 (8)
	z	4862	14 (1)	12 (4)	−12 (4)	
Zn	x	2500	−54 (8)	35 (2)	108 (2)	
	y	4217	−1 (1)	5 (4)	−21 (3)	779 (9)
	z	2240	−12 (1)	−3 (5)	14 (5)	
Cl(1)	x	2500	−93 (12)	100 (10)	503 (8)	
	y	4189	17 (2)	−59 (7)	−44 (8)	220 (21)
	z	−175	−19 (2)	−13 (8)	57 (9)	
Cl(2)	x	2500	−60 (9)	647 (6)	86 (10)	
	y	5851	−10 (2)	8 (8)	−33 (5)	169 (20)
	z	3204	28 (2)	4 (10)	9 (7)	
Cl(3)	x	10	−70 (9)	−249 (9)	69 (8)	
	y	3410	−3 (5)	341 (7)	−18 (5)	215 (23)
	z	3139	−37 (6)	208 (8)	−114 (7)	
Cl(4)	x	4990	−81 (9)	−244 (9)	44 (8)	
	y	3410	−48 (4)	−321 (7)	−9 (5)	204 (23)
	z	3139	−14 (6)	−126 (8)	115 (7)	

* Not refined to fix the origin.

5. Discussion

Several other modulated structure determinations of A_2BX_4 compounds have been performed by different authors: K_2SeO_4 (Yamada & Ikeda, 1984), $[N(CH_3)_4]_2CoCl_4$ (Fjaer, 1985), $[N(CH_3)_4]_2ZnCl_4$ (Madariaga, Zuñiga, Pérez-Mato & Tello, 1987), and Rb_2ZnBr_4 (Hogervorst & Helmholdt, 1988). Consequently, it is interesting to compare the common features of these structures in order to clarify the processes of the phase transitions at T_i and T_L.

The most striking common feature is the rigid-body behaviour, to a good approximation, of the BX_4 tetrahedra. This is outlined by the weak variations of the interatomic distances B–X and X–X of a tetrahedron (Table 5), which are much smaller than the modulated displacements of the respective atoms. The comparison of these distances in the case of the ZnX_4 tetrahedra (with X = Cl or Br) reveals common features and analogous geometries in the different structural refinements. The B–$X(1)$ distance is the shortest and the most rigid one. The atom $X(3)$ is responsible for the larger fluctuations, and this can be correlated with the fact that it is the only atom in a general position with no symmetry restriction on its modulation functions.

The modulated displacements of X atoms from their average positions are then treated as rotations around the crystallographic axes, the strongest being generally around the pseudo-hexagonal axis. The calculated

Table 5. *Interatomic distances* (Å) *inside* BX_4 *tetrahedra for* A_2BX_4 *compounds*

	BX_1	BX_2	BX_3	X_1X_2	X_1X_3	X_2X_3	X_3X_4
Rb_2ZnCl_4							
d_{min}	2·228	2·247	2·234	3·763	3·651	3·571	3·604
d_{max}	2·242	2·280	2·276	3·807	3·730	3·676	3·676
%	0·6	1·5	1·9	1·2	2·2	2·9	2·0
Rb_2ZnBr_4							
d_{min}	2·368	2·384	2·368	3·992	3·888	3·806	3·850
d_{max}	2·377	2·415	2·421	4·031	3·949	3·884	3·911
%	0·3	1·3	2·2	1·0	1·5	2·0	1·6
TMA_2ZnCl_4							
d_{min}	2·188	2·273	2·224	3·726	3·580	3·630	3·712
d_{max}	2·191	2·287	2·296	3·737	3·667	3·680	3·741
%	0·1	0·6	3·3	0·3	2·4	1·4	0·8

values in our case, 10° around z and 5° around y, are a little larger than in other compounds. The pseudo-hexagonal axis (the **c** axis in Rb_2ZnCl_4) corresponds to the sixfold screw axis of a latent hexagonal phase, by analogy with K_2SeO_4. Based on the work of Katkanant, Edwardson, Hardy & Boyer (1986), the existence of this imperfect hexagonal symmetry should be the origin of the incommensurate behaviour. Our calculations of rotations of $ZnCl_4$ tetrahedra are in agreement with their description of the incommensurate phase which consists in decomposing the transformation at T_i into two components similar to R_y and R_z rotations, the strongest rotational displacements (R_z) costing no energy. This result and the phase relations between the rotations of tetrahedra are common for all the compounds studied except K_2SeO_4 (Yamada & Ikeda, 1984), where $R_y = 7$ and $R_z = 4°$.

The rotations of the BX_4 tetrahedra are associated with a translational motion along the **a** direction. In Rb_2ZnCl_4, the maximum translation of the rigid-body $ZnCl_4$ is 0·11 Å; in the TMA system, the larger translation {0·21 Å for $[N(CH_3)_4]_2CoCl_4$} is certainly related to the larger size of the **a** parameter.

Another common feature between the different studies is the similarity of the modulation and the structural description in the INC and C phases. The rotational angles of $ZnCl_4$ tetrahedra increase a little but a constant ratio is maintained between R_y and R_z (Fig. 5). Thus at the lock-in phase transition there is no discontinuity with regard to the modulation-function amplitudes and the BX_4 rotations. Nevertheless, the two compared structures have been refined at two very different temperatures, for which they are well characterized and for which the crystal periodicities of the basic lattice and of the modulation are defined with a long-range order (sharpness of the diffraction reflections). The intermediate temperatures are characterized by the coexistence of different phases or by the appearance of domains and discommensurations. These are the result of the rapid evolution and of the discontinuity at T_L of the modulus of the modulation vector. This involves a sudden shift of the internal phase, and hence a sudden displacement of the atoms near T_L.

In A_2BX_4 compounds, the incommensurability is connected with the ferroelectric properties of the crystal.

Several studies based on polarization measurements in Rb_2ZnCl_4 have shown the existence of a polarization along the **a** direction which is reduced to zero above T_L (Sawada *et al.*, 1977; Shuvalov *et al.*, 1988). Consequently, calculations of polarization were performed from the structural results of the INC and C phases. We have considered that the electric charge +2e is localized at the centre of the Rb(1)—Rb(2) ionic pair and −2e at the centre of gravity of the respective tetrahedra (which is theoretically the Zn atom). These calculations have pointed out a local polarization in one cell (Fig. 7), its average over three cells being almost but not exactly reduced to zero. Other calculations were performed using the structural results of a refinement in a noncentrosymmetric superspace group $P(P2_1cn)$: $(\bar{1},s,\bar{1})$. They resulted in a strong polarization (0·5 μC cm^{-2}) larger than the calculated one for the C phase and in disagreement with all the polarization measurements. Consequently, the hypothesis of a centrosymmetric group in the INC phase is confirmed in spite of the weaker values of final wR factors obtained in the noncentrosymmetric hypothesis.

In the lock-in phase a spontaneous polarization was determined along the **a** direction. Its value (0·39 μC cm^{-2}) corresponds approximately to the measurements performed by Hamano *et al.* (1980) and results from the shift of the average positions of Rb(1) atoms (Table 4). These results are in agreement with a similar study of K_2SeO_4 (Yamada, Ono & Ikeda, 1984). They show the particular role of Rb(1) atoms which have anomalously large thermal motions in the INC and C phases. This effect, which is certainly due to the large cage of Cl atoms around Rb(1), is observed in Rb_2ZnBr_4 (Hogervorst & Helmholdt, 1988) and K_2SeO_4 (Yamada & Ikeda, 1984) and shows that the ferroelectricity essentially depends on average atomic positions.

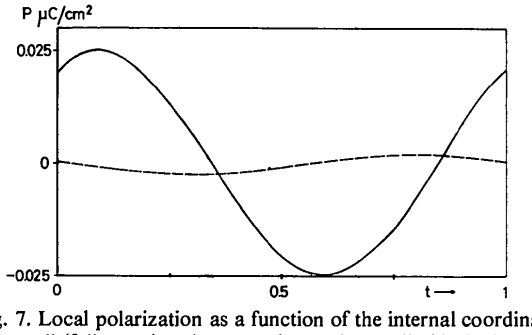

Fig. 7. Local polarization as a function of the internal coordinate in one cell (full curve) and averaged over three cells (dashed curve).

Yamada & Hamaya (1983) have compared two groups of A_2BX_4 compounds: A_2ZnX_4 materials (A = K, Rb, NH_4; X = Cl, Br) and $(TMA)_2MCl_4$ materials [TMA = $N(CH_3)_4$, M = Zn, Cu, Co, Fe, Ni] which present different INC–C successive phase transitions. In the first group, the temperature range of the INC phase is relatively wide and the incommensurate wavevector decreases as the temperature decreases, and locks into $q = 1/3$. In the second group, the modulation wavevectors tend to increase with decreasing temperature, the lock-in wavevectors take several values (2/5, 1/2, 1/3) and the temperature range of the INC phases is reduced. With an *EXAF*II model, Yamada & Hamaya (1983) have shown that A_2ZnX_4 compounds are characterized by relatively small second- and third-neighbour interactions, opposite to observations of $(TMA)_2MCl_4$ compounds. These results are in agreement with the fact that Rb–Cl interatomic distances and their variations are very similar to the Rb–Br ones (Hogervorst & Helmholdt, 1988), given the difference between the ionic radii of Cl and Br atoms, and the INC phases of these two compounds are really isostructural. In contrast, the TMA–Cl distances and their variations are relatively stronger than the Rb–X ones, whereas the M–Cl distances in a tetrahedron are similar in both groups. These results may be related to the difference between the cell parameters of the two families and may explain the existence of two different types of INC structures and of two different INC–C phase-transition processes. From these considerations, the hypothesis can be made of two families of isostructural A_2BX_4 compounds, which must be confirmed by further structural studies.

References

FJAER, E. (1985). *Acta Cryst.* **B41**, 330–336.

FOUSEK, J. & KROUPA, J. (1987). *Solid State Commun.* **63**(9), 769–772.

GREBILLE, D., WEIGEL, D., VEYSSEYRE, R. & PHAN, T. (1989). In preparation.

HAMANO, K., IKEDA, Y., FUJIMOTO, T., EMA, K. & HIROTSU, S. (1980). *J. Phys. Soc. Jpn,* **49**(6), 2278–2286.

HAMANO, K., SAKATA, H. & EMA, K. (1985). *J. Phys. Soc. Jpn,* **54**(5), 2021–2031.

HEDOUX, A., GREBILLE, D., LEFEBVRE, J. & PERRET, R. (1989). *Phase Transitions,* **14**, 177–186.

HOGERVORST, A. C. R. & HELMHOLDT, R. B. (1988). *Acta Cryst.* **B44**, 120–128.

International Tables for X-ray Crystallography (1974). Vol. IV. Birmingham: Kynoch Press. (Present distributor Kluwer Academic Publishers, Dordrecht.)

KATKANANT, V., EDWARDSON, P. J., HARDY, J. R. & BOYER, L. L. (1986). *Phys. Rev. Lett.* **57**(16), 2033–2036.

KATO, N. (1976*a*). *Acta Cryst.* **A32**, 453–457.

KATO, N. (1976*b*). *Acta Cryst.* **A32**, 458–466.

MADARIAGA, G., ZUÑIGA, F. J., PÉREZ-MATO, J. M. & TELLO, M. J. (1987). *Acta Cryst.* **B43**, 356–368.

QUILICHINI, M. & PANNETIER, J. (1983). *Acta Cryst.* **B39**, 657–663.

SAWADA, S., SHIROISHI, Y., YAMAMOTO, A., TAKASHIGE, M. & MATSUO, M. (1977). *J. Phys. Soc. Jpn,* **43**(6), 2099–2100.

SHUVALOV, L. A., GRIDNEV, S. A., PRASOLOV, B. N. & SANNIKOV, V. G. (1988). *Fiz. Tverd. Tela (Leningrad),* **30**(2), 620–622.

WOLFF, P. M. DE, JANSSEN, T. & JANNER, A. (1981). *Acta Cryst.* **A37**, 625–636.

YAMADA, N. & IKEDA, T. (1984). *J. Phys. Soc. Jpn,* **53**(8), 2555–2564.

YAMADA, N., ONO, Y. & IKEDA, T. (1984). *J. Phys. Soc. Jpn,* **53**(8), 2565–2574.

YAMADA, Y. & HAMAYA, N. (1983). *J. Phys. Soc. Jpn,* **52**(10), 3466–3474.

YAMAMOTO, A. (1982). *REMOS.* Computer program for the refinement of modulated structures. National Institute for Research in Inorganic Materials, Niihari-gun, Ibaraki, Japan.

Acta Cryst. (1989). **B45**, 378–383

Molecular Volumes and Packing Efficiency. An Approach to Metal Cluster Properties in the Solid State

BY DARIO BRAGA* AND FABRIZIA GREPIONI

Dipartimento di Chimica 'G. Ciamician', Università di Bologna, Via Selmi 2, 40126 *Bologna, Italy*

(*Received* 28 *November* 1988; *accepted* 1 *March* 1989)

Abstract

Molecular volumes, surfaces and packing coefficients are calculated, starting from known crystal structures, for a number of neutral metal-carbonyl clusters by applying the method of intersecting caps widely used in organic solid-state chemistry. The problem of an appropriate atomic radius attribution is discussed. The results of the packing analysis are used to investigate the relationship between packing efficiency and occurrence of dynamic processes in the solid state, as well as many structural properties of metal-carbonyl clusters.

* To whom correspondence should be addressed.

0108-7681/89/040378-06$03.00 © 1989 International Union of Crystallography

Introduction

Although the concept of molecular shape has been diffusely applied to the analysis of transition-metal